

Coherent Storage of Microwave Excitations in Rare-Earth Nuclear Spins

Gary Wolfowicz,^{1,2} Hannes Maier-Flaig,^{1,*} Robert Marino,^{3,4} Alban Ferrier,^{3,5} Hervé Vezin,⁴
John J. L. Morton,^{1,6} and Philippe Goldner^{3,†}

¹*London Centre for Nanotechnology, University College London, London WC1H 0AH, United Kingdom*

²*Department of Materials, Oxford University, Oxford OX1 3PH, United Kingdom*

³*PSL Research University, Chimie ParisTech–CNRS, Institut de Recherche de Chimie Paris, 75005, Paris, France*

⁴*LASIR CNRS UMR 8516, Université de Lille, France*

⁵*Sorbonne Universités, UPMC Univ Paris 06, 75005, Paris, France*

⁶*Department of Electronic and Electrical Engineering, UCL, London WC1E 7JE, United Kingdom*

(Received 19 December 2014; published 30 April 2015)

Interfacing between various elements of a computer—from memory to processors to long range communication—will be as critical for quantum computers as it is for classical computers today. Paramagnetic rare-earth doped crystals, such as $\text{Nd}^{3+}:\text{Y}_2\text{SiO}_5$ (YSO), are excellent candidates for such a quantum interface: they are known to exhibit long optical coherence lifetimes (for communication via optical photons), possess a nuclear spin (memory), and have in addition an electron spin that can offer hybrid coupling with superconducting qubits (processing). Here we study two of these three elements, demonstrating coherent storage and retrieval between electron and ^{145}Nd nuclear spin states in $\text{Nd}^{3+}:\text{YSO}$. We find nuclear spin coherence times can reach 9 ms at ~ 5 K, about 2 orders of magnitude longer than the electron spin coherence, while quantum state and process tomography of the storage or retrieval operation between the electron and nuclear spin reveal an average state fidelity of 0.86. The times and fidelities are expected to further improve at lower temperatures and with more homogeneous radio-frequency excitation.

DOI: [10.1103/PhysRevLett.114.170503](https://doi.org/10.1103/PhysRevLett.114.170503)

PACS numbers: 03.67.Lx, 03.67.Hk, 76.30.Kg, 76.70.Dx

Hybrid quantum systems composed of spin ensembles strongly coupled to superconducting resonators have recently emerged as a promising route for quantum memories operating in the microwave regime [1,2]. Such memories offer the possibility exploiting electron spin coherence times of up to seconds [3] as a resource for superconducting qubits, whose coherence times so far extend only to tens of microseconds [4]. Strong coupling has been observed between superconducting resonators and various paramagnetic impurities, including NV centers in diamond [5] and erbium ions in Y_2SiO_5 (YSO) and YAlO_3 [6–8], leading to reversible coherent storage of (large numbers of) microwave photons within spin ensembles [9,10]. These paramagnetic impurities are often coupled to nuclear spins that can offer a further resource for storage—electronic spin coherences can be transferred to and from a nuclear spin [11–13], to access coherence times as long as hours [14].

The proposal to use solid-state spin ensembles as microwave quantum memories is in many ways inspired by results on using impurities in solid for optical quantum memories [15,16], where optical excitations are stored in rare-earth (RE) nuclear spins [17–20]. Very long storage time can be expected, as nuclear spin coherence lifetimes in such materials extend up to 6 h [21]. Entanglement storage [22] and light-matter teleportation at telecom wavelength [23] have been demonstrated in $\text{Nd}^{3+}:\text{Y}_2\text{SiO}_5$, for which optical coherence lifetimes of 90 μs have been measured [24,25].

Bringing together both optical and microwave strong coupling techniques on the same ensemble would enable a versatile quantum interface, connecting quantum memory, processing, and communication and potentially allowing faithful conversion of microwave to optical photons [26,27]. However, hyperfine coherence lifetimes T_{2n} have been so far only measured for RE ions with an even number of f electrons and no electron spin [28–31]. For paramagnetic RE ions, an electromagnetically induced transparency experiment showed that $T_{2n} > 0.4 \mu\text{s}$ in $^{167}\text{Er}^{3+}:\text{YSO}$ at 1.5 K and zero magnetic field [32]. Since superconducting qubits can have coherence lifetimes of several tens of μs [4], it is therefore unknown whether nuclear spins could still provide a memory resource in the case of paramagnetic RE ions, which are required for coupling to microwave excitations. In this Letter we study a paramagnetic RE doped crystal $\text{Nd}^{3+}:\text{Y}_2\text{SiO}_5$ and measure electron and nuclear spin coherence times of up to 100 μs and 9.2 ms, respectively. We further demonstrate coherence transfer between electron and nuclear spin degrees of freedom in the Nd^{3+} ion—quantum state and process tomography show transfer fidelities above the classical limit. These results suggest that quantum memories for microwave photons with access to long storage times are achievable in rare-earth doped crystals.

Y_2SiO_5 (YSO) is a monoclinic crystal (C_{2h}^6 space group) with two crystallographic sites of C_1 symmetry for Y^{3+} ions, which can be substituted by Nd^{3+} ions [Fig. 1(a)].

Each site is divided in two classes related by a C_2 symmetry along the crystal b axis. For magnetic fields parallel or perpendicular to the b axis, ions in the two classes are magnetically equivalent. Nd^{3+} has a $[\text{Xe}]4f^3$ electronic configuration, with a $^4I_{9/2}$ ground multiplet. In C_1 symmetry, the crystal field (CF) splits the J multiplets into twofold degenerate levels. At low temperature, only the lowest doublet is populated and the system can be considered as an effective $S = 1/2$ spin. Nd^{3+} has two isotopes with a $I = 7/2$ nuclear spin, ^{143}Nd and ^{145}Nd , with respective natural abundance of 12.2% and 8.3%, as well as 5 isotopes with zero nuclear spin. To reduce the concentration of ions not involved in the storage experiments and potentially causing dephasing, an isotopically pure crystal boule of 0.001 at. % $^{145}\text{Nd}:\text{YSO}$ was grown by the Czochralski method. Samples of about 1.5 mm^3 were cut with faces perpendicular to the b , $D1$, and $D2$ principal axes of the optical indicatrix. Experiments were performed using an X-band (9.7 GHz) Bruker electron spin resonance (ESR) spectrometer (Elexys 580) equipped with a helium cryostat. Microwave (mw) π pulses were 32 ns long and radio-frequency (rf) pulses about 3 μs .

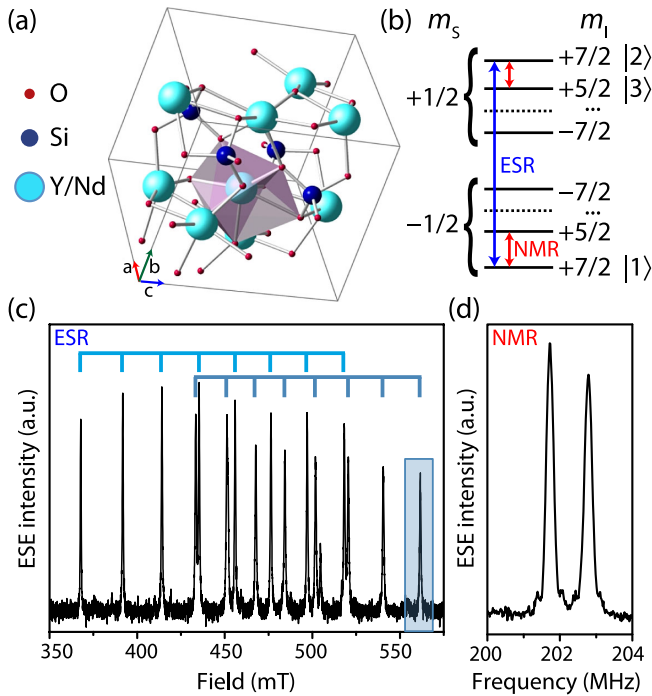


FIG. 1 (color online). (a) Y_2SiO_5 crystal structure showing the coordination polyhedron corresponding to Nd^{3+} site within a unit cell. (b) Schematic energy level diagram of $^{145}\text{Nd}^{3+}$ ions highlighting relevant electron and nuclear spin transitions in blue and red, respectively. (c) Field swept ESE spectrum for a magnetic field close to $D1$ ($T = 6.5 \text{ K}$) showing two sets of ESR transitions from two magnetically inequivalent Nd^{3+} classes. The electron spin transition at 561.5 mT was used for all ENDOR experiments, such as the spectrum shown in (d).

Figure 1(c) shows the field swept electron spin echo (ESE) spectrum obtained for a magnetic field oriented close to the $D1$ axis. The 16 intense lines correspond to the allowed ESR transitions ($\{\Delta m_I, \Delta m_S\} = \{0, \pm 1\}$) for the two magnetically inequivalent classes of one site. For some orientations of the magnetic field, weaker lines corresponding to $I = 0$ isotopes in the same site were observed. These results suggest that Nd^{3+} ions preferentially occupy one of the Y^{3+} crystallographic sites. The full linewidth at half maximum of the transition at 561.5 mT is 12 MHz, which is comparable to the narrowest linewidths measured in $\text{Er}^{3+}:\text{YSO}$, recently used to demonstrate strong coupling to a superconducting resonator [6]. All ENDOR and relaxation experiments below were performed at 561.5 mT. The Zeeman g and hyperfine A tensors were determined from CW spectra obtained by rotating the sample in planes containing the static magnetic field and perpendicular to the $D1$, $D2$, and b axes. A least squares fit to the ESR line positions gives the principal values of the g tensor (see Supplemental Material [33]): $g_x = 1.49$, $g_y = -0.98$, $g_z = -4.17$ with the Euler angles ($z x z$ convention) relating the principal axes to the crystal axes $D1$, $D2$, and b : $\alpha = 192^\circ$, $\beta = 39^\circ$, and $\gamma = 183^\circ$. In the same reference axes, the principal values of A and the corresponding Euler angles are $A_x = 398$, $A_y = 0.1$, $A_z = 827 \text{ MHz}$, and $\alpha = 154^\circ$, $\beta = 34^\circ$, and $\gamma = 200^\circ$. As expected in low symmetry, the g and A tensors are highly anisotropic, but their principal axes are nearly parallel, as was observed for site 1 in $\text{Er}^{3+}:\text{YSO}$ [34].

An electron-nuclear double resonance (ENDOR) spectrum was recorded [Fig. 1(d)], using a Davies ENDOR sequence with Tidy pulse [35,36]. The two ENDOR lines located at 201.7 and 202.8 MHz have Gaussian shapes with linewidths of 235 and 248 kHz, respectively. Simulations confirm that these correspond to $+5/2: +7/2$ transitions in m_I , where the lower (higher) frequency line corresponds to the $m_S = +1/2$ ($m_S = -1/2$) transition. The coherence storage experiments described below involve the three transitions labeled $|1\rangle \dots |3\rangle$ as shown in Fig. 1(b).

The electron spin population relaxation time, T_{1e} , was measured by an inversion-recovery sequence as a function of temperature between 5 and 7 K. T_{1e} increases with decreasing temperature from 0.1 to 30 ms (Fig. 2) and can be modeled above 5.5 K by an Orbach process with a CF level located 77 cm^{-1} above the ground state, in reasonable agreement with the value of 88 cm^{-1} deduced from optical measurements [37]. The electron spin coherence lifetime T_{2e} was also studied in the same temperature range (Fig. 2), yielding stretched exponential decays with T_{2e} increasing from 28 to 106 μs with decreasing temperature. Stretched factors ranged between 1.2 and 1.5 below 6 K. We attribute the strong temperature dependence in T_{2e} to the effect of spectral diffusion resulting from interactions with a bath of electrons spins undergoing spin relaxation [38,39]. When the bath relaxation rate is much larger than the echo measurement scale, a stretch factor of ≈ 1.5 indicates a

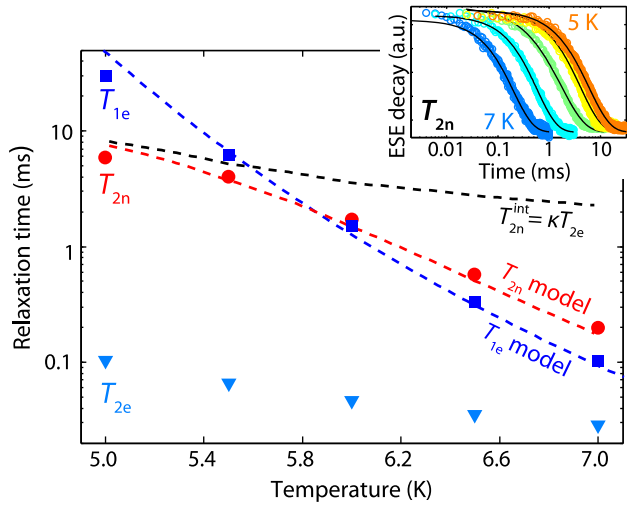


FIG. 2 (color online). Electron and nuclear spin relaxation times as a function of temperature: T_{1e} (squares), T_{2e} (triangles), and T_{2n} (circles). In the inset, corresponding decay curves for T_{2n} from 5 to 7 K. T_{1e} is modeled with an Orbach process $1/T_{1e} = A \exp(-\Delta E/k_B T)$ with $A = 6 \times 10^{10} \text{ s}^{-1}$ and $\Delta E = 77 \text{ cm}^{-1}$ (k_B is the Boltzmann constant). T_{2n} is limited by $2T_{1e}$ giving the relation $1/T_{2n} = 1/(2T_{1e}) + 1/T_{2n}^{\text{int}}$, where T_{2n}^{int} is the decay time for the nucleus due to the spin environment only. As this decay has the same origin as for the electron, we can simply relate $T_{2n}^{\text{int}} = \kappa T_{2e}$.

Gaussian diffusion process [39]. Using this model and taking Nd^{3+} ions themselves as the spin bath, T_{2e} can be estimated from T_{1e} , the effective $g = 1.5$ and Nd^{3+} concentration ($9.4 \times 10^{16} \text{ ions/cm}^3$), which gives $T_{2e} = 471 \mu\text{s}$. This is about 4 times longer than the measured value and can be explained by the anisotropy of the g tensor, which increases the dipole-dipole interaction [40]. Angular variation in the $D1 - D2$ plane showed that T_{2e} is maximal in a region of about 5° around $D1$ axis and decreases by a factor of 2 at lower resonance fields.

Transfer between electron and nuclear spin coherences was performed using the sequence shown in Fig. 3(a) [11], which is fully compatible with the schemes designed for single photon operation [1,2]. In our experiments, the memory input is a $\pi/2$ microwave pulse [consisting of $\mathcal{O}(10^{17})$ photons]. It creates an electron spin coherence on the $|1\rangle:|2\rangle$ transition, which is then refocused by a π pulse to remove the effect of inhomogeneous broadening. Before refocusing is complete, an rf π pulse on the $|2\rangle:|3\rangle$ transition transfers the coherence to $|1\rangle:|3\rangle$. At the time when this transition refocuses, a mw π pulse transfers the electron spin coherence to the $|2\rangle:|3\rangle$ NMR transition. To retrieve the coherent microwave signal from the nuclear spin ensemble, an rf π pulse refocuses the $|2\rangle:|3\rangle$ coherence, and then the sequence described above is applied in reverse order. A final mw π produces an electron spin echo, which is the output of the memory. This scheme allows extending storage times beyond T_{2e} , limited instead by the nuclear spin coherence time T_{2n} .

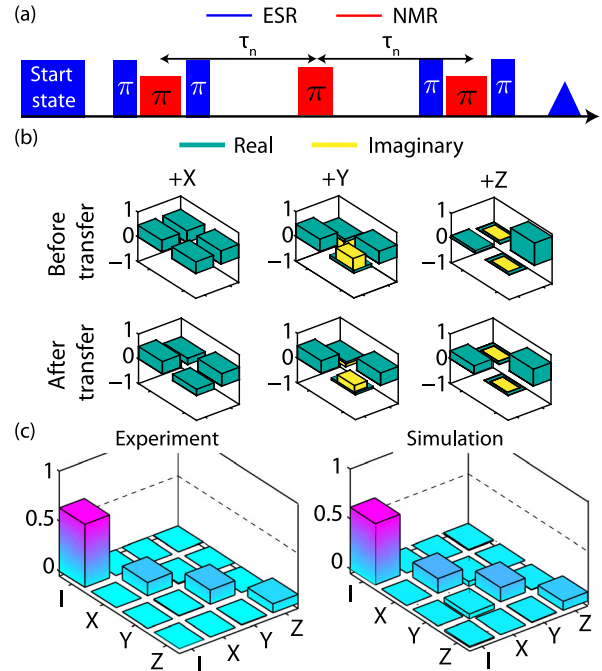


FIG. 3 (color online). (a) Sequence used for storing mw photons into nuclear spin coherences. (b) Input $+\sigma_X$, $+\sigma_Y$, and $+\sigma_Z$ (upper row) and corresponding output (lower row) density matrices are obtained by state tomography. Real and imaginary parts are shown in green and yellow, respectively. (c) Quantum process tomography matrix χ in the $(1, \sigma_X, \sigma_Y, \sigma_Z)$ basis. A perfect storage process would give only a $[1, 1]$ component. Left: Matrix reconstructed from experimental density matrices. Right: Simulated matrix considering pulse fidelity and spin relaxations.

T_{2n} was measured by monitoring the output echo amplitude as a function of $2\tau_n$ in the storage sequence [Fig. 3(a)]. Echo decays were nearly exponential with maximal stretch factors of 1.25 and ranged from 184 μs at 7 K to 6 ms at 5 K (Fig. 2). T_{2n} is bounded by $2T_{1e}$ when there is significant hyperfine coupling [11], and this limit is indeed observed for temperatures above 6 K. Below this temperature, some intrinsic nuclear spin decoherence mechanism is evident. We assume this intrinsic T_{2n} follows the measured electron spin decoherence time T_{2e} , adjusted by some factor κ to reflect the ratio of the effective g factors for those ESR and NMR transitions: i.e., $1/T_{2n} = 1/(2T_{1e}) + 1/(\kappa T_{2e})$. T_{2n} was found to depend significantly on the nuclear transition probed as well as on the static magnetic field orientation and ranged from 1.5 to 9.2 ms at 5 K, which can be understood by variations in κ .

We next examine the fidelity of the storage and retrieval process between the electron spin degree of freedom and the ^{145}Nd nuclear spin, using quantum state tomography and quantum process tomography at 6.5 K to avoid low repetition rates due to the long T_{1e} . The overall fidelity for quantum memory of microwave and/or optical photons will additionally depend on the fidelity of the collective excitation of the ensemble—this is not studied here, but

current state of the art shows fidelities of $\sim 14\%$ for microwave memories [41], while for optical ones, 87% [42] has been achieved in an atomic vapor and 69% in a rare-earth doped crystal [43]. Quantum state tomography is performed by measuring the qubit state in the Pauli basis $(\sigma_X, \sigma_Y, \sigma_Z)$. Components σ_X and σ_Y are simply the real and imaginary part of the electron spin echo, while σ_Z can be measured by an additional $\pi/2$ pulse immediately following the echo, to map σ_Z onto σ_X [11]. To obtain the overall process matrix of the electron-nuclear-electron spin transfer, density matrices are measured for the set of electron spin input states: $\pm\sigma_X$, $\pm\sigma_Y$, $\pm\sigma_Z$, and 1 [Fig. 3(b)]. We are interested in obtaining the process matrix for the storage or retrieval operation itself, and so reference the output states against a simple two-pulse electron spin echo experiment with total duration equal to the time the coherent state resides in the electron spin degree of freedom, in the actual transfer sequence. In this way, losses related to electron spin relaxation, dephasing, and state preparation are partly taken into account, but not errors related to the nuclear spin. The input and output states for the memory process are then linked by the relation, for a spin 1/2:

$$\epsilon(\rho_{\text{end}}) = \sum_{m,n=0}^3 \chi_{mn} A_m \rho_{\text{start}} A_n^\dagger, \quad (1)$$

where χ is the process matrix that is reconstructed, A the operators from the Pauli basis $(1, \sigma_X, \sigma_Y, \sigma_Z)$, and ρ_{start} and ρ_{end} the input and output density matrices (for a particular electron spin initial state) [44,45].

We measure an average state fidelity [where $F_{\text{state}} = \text{Tr}(\sqrt{\sqrt{\rho_{\text{end}}}\rho_{\text{start}}\sqrt{\rho_{\text{end}}}})^2$] of $\overline{F_{\text{state}}} = 0.86$, compared to what we would expect for an ideal memory, well above the classical limit of $2/3$ [46]. The computed process matrix χ is shown in Fig. 3(c) and we find a process fidelity $F_p = \text{Tr}(\chi\chi_{\text{ideal}}) = 0.63$, where χ_{ideal} has just the identity component. Typically, average state and process fidelities are related by $\overline{F_{\text{state}}} = (2F_p + 1)/3 = 0.75$ for a pure spin-1/2 [47]. However, preparation and measurements are realized here on the electron spin, but are conditional on a particular nuclear spin state, and so the reconstructed states do not span the full electron spin-1/2 state space. The reconstructed χ process matrix was well simulated using a Linblad master equation and taking into account electron and nuclear spin relaxation rates (T_{1e} , T_{2e} , and T_{2n}), as well as pulse inhomogeneities [Fig. 3(c)]. The latter were determined from fits to measured electron and nuclear spin Rabi oscillations (Fig. 4). The main process errors can be assigned to two particular contributions: first, the low fidelity of the rf pulses results in the large components in the $[\sigma_X, \sigma_X]$ and $[\sigma_Y, \sigma_Y]$ part of χ . Use of concatenated or adiabatic pulses would be expected to significantly address this issue [48,49]. The second contribution is pure dephasing, as evidenced by the $[\sigma_Z, \sigma_Z]$ component in χ , and is due to electron coherence decay during the application of the rf

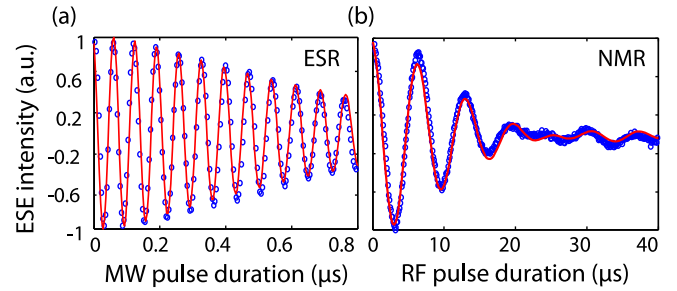


FIG. 4 (color online). (a) Electron Rabi oscillations obtained on the $|1\rangle:|2\rangle$ transition [Fig. 1(b)]. The decay is Gaussian, typical of mw pulse inhomogeneity, with a standard deviation about 1.5% of the Rabi frequency. (b) Nuclear Rabi oscillations obtained on the $|2\rangle:|3\rangle$ transition. The oscillations do not decay completely and can be modeled by the use of a truncated Gaussian for the rf pulse inhomogeneity. Such behavior is likely due to the small sample size which only sees part of the magnetic field inhomogeneity (nearly 14% here) from the rf coil.

pulse. This could be significantly improved by lowering the temperature to increase T_{2e} (Fig. 2).

In conclusion, we have shown that microwave excitations can be stored into a nuclear spin coherence in an isotopically pure rare-earth doped crystal, $^{145}\text{Nd}^{3+}:\text{Y}_2\text{SiO}_5$. Storage times, determined by the nuclear coherence lifetime, can reach 9.2 ms, about 2 orders of magnitude longer than the electron spin T_{2e} and the best superconducting qubit coherence times. Furthermore, these storage times could be significantly increased by dynamical decoupling techniques [11]. Given their long optical coherence lifetimes, our results show that paramagnetic rare-earth doped crystals could be used as long-lived quantum memories to interface superconducting qubits with both microwave and optical qubits.

The authors thank M. Afzelius for useful discussions. This work received funding from the European Union's Seventh Framework Programme FP7/2007-2013/ under REA Grant Agreements No. 287252 (CIPRIS, People Programme-Marie Curie Actions), No. 247743 (QuRep), and No. 279781 (ASCENT), Idex ANR-10-IDEX-0001-02 PSL and Région Nord-Pas-de-Calais. Work at UCL is supported by the EPSRC through a DTA and the Materials World Network (EP/I035536/1). J. J. L. M. is supported by the Royal Society.

*Present address: Walther-Meissner-Institut, Bayerische Akademie der Wissenschaften, 85748 Garching, Germany.
†philippe.goldner@chimie-paristech.fr

- [1] B. Julsgaard, C. Grezes, P. Bertet, and K. Mølmer, *Phys. Rev. Lett.* **110**, 250503 (2013).
- [2] M. Afzelius, N. Sangouard, G. Johansson, M. U. Staudt, and C. M. Wilson, *New J. Phys.* **15**, 065008 (2013).
- [3] G. Wolfowicz, A. M. Tyryshkin, R. E. George, H. Riemann, N. V. Abrosimov, P. Becker, H.-J. Pohl, M. L. W. Thewalt, S. A. Lyon, and J. J. L. Morton, *Nat. Nanotechnol.* **8**, 561 (2013).

- [4] C. Rigetti, J. M. Gambetta, S. Poletto, B. L. T. Plourde, J. M. Chow, A. D. Córcoles, J. A. Smolin, S. T. Merkel, J. R. Rozen, G. A. Keefe, M. B. Rothwell, M. B. Ketchen, and M. Steffen, *Phys. Rev. B* **86**, 100506 (2012).
- [5] Y. Kubo, F. R. Ong, P. Bertet, D. Vion, V. Jacques, D. Zheng, A. Dréau, J. F. Roch, A. Auffèves, F. Jelezko, J. Wrachtrup, M. F. Barthe, P. Bergonzo, and D. Esteve, *Phys. Rev. Lett.* **105**, 140502 (2010).
- [6] S. Probst, H. Rotzinger, S. Wünsch, P. Jung, M. Jerger, M. Siegel, A. V. Ustinov, and P. A. Bushev, *Phys. Rev. Lett.* **110**, 157001 (2013).
- [7] A. Tkalcec, S. Probst, D. Rieger, H. Rotzinger, S. Wünsch, N. Kukharchyk, A. D. Wieck, M. Siegel, A. V. Ustinov, and P. Bushev, *Phys. Rev. B* **90**, 075112 (2014).
- [8] S. Probst, H. Rotzinger, A. V. Ustinov, and P. A. Bushev, [arXiv:1501.01499](https://arxiv.org/abs/1501.01499).
- [9] Y. Kubo, I. Diniz, A. Dewes, V. Jacques, A. Dréau, J. F. Roch, A. Auffèves, D. Vion, D. Esteve, and P. Bertet, *Phys. Rev. A* **85**, 012333 (2012).
- [10] X. Zhu, S. Saito, A. Kemp, K. Kakuyanagi, S.-i. Karimoto, H. Nakano, W. J. Munro, Y. Tokura, M. S. Everitt, K. Nemoto, M. Kasu, N. Mizuochi, and K. Semba, *Nature (London)* **478**, 221 (2011).
- [11] J. J. L. Morton, A. M. Tyryshkin, R. M. Brown, S. Shankar, B. W. Lovett, A. Ardavan, T. Schenkel, E. E. Haller, J. W. Ager, and S. A. Lyon, *Nature (London)* **455**, 1085 (2008).
- [12] R. M. Brown, A. M. Tyryshkin, K. Porfyakis, E. M. Gauger, B. W. Lovett, A. Ardavan, S. A. Lyon, G. A. D. Briggs, and J. J. L. Morton, *Phys. Rev. Lett.* **106**, 110504 (2011).
- [13] H. Wu, R. E. George, J. H. Wesenberg, K. Mølmer, D. I. Schuster, R. J. Schoelkopf, K. M. Itoh, A. Ardavan, J. J. L. Morton, and G. A. D. Briggs, *Phys. Rev. Lett.* **105**, 140503 (2010).
- [14] K. Saeedi, S. Simmons, J. Z. Salvail, P. Dluhy, H. Riemann, N. V. Abrosimov, P. Becker, H. J. Pohl, J. J. L. Morton, and M. L. W. Thewalt, *Science* **342**, 830 (2013).
- [15] W. Tittel, T. Chanelière, R. L. Cone, S. Kröll, S. A. Moiseev, and M. J. Sellars, *Laser Photonics Rev.* **4**, 244 (2010).
- [16] P. Goldner, A. Ferrier, and O. Guillot-Noël, in *Handbook on the Physics and Chemistry of Rare Earths*, edited by J.-C. G. Bünzli and V. K. Pecharsky (Elsevier B.V., Amsterdam, 2015), Vol. 46, p. 1.
- [17] J. J. Longdell, E. Fraval, M. J. Sellars, and N. B. Manson, *Phys. Rev. Lett.* **95**, 063601 (2005).
- [18] M. Afzelius, I. Usmani, A. Amari, B. Lauritzen, A. Walther, C. Simon, N. Sangouard, J. Minář, H. de Riedmatten, N. Gisin, and S. Kröll, *Phys. Rev. Lett.* **104**, 040503 (2010).
- [19] M. Lovrić, D. Suter, A. Ferrier, and P. Goldner, *Phys. Rev. Lett.* **111**, 020503 (2013).
- [20] G. Heinze, C. Hubrich, and T. Halfmann, *Phys. Rev. Lett.* **111**, 033601 (2013).
- [21] M. Zhong, M. P. Hedges, R. L. Ahlefeldt, J. G. Bartholomew, S. E. Beavan, S. M. Wittig, J. J. Longdell, and M. J. Sellars, *Nature (London)* **517**, 177 (2015).
- [22] C. Clausen, I. Usmani, F. Bussières, N. Sangouard, M. Afzelius, H. de Riedmatten, and N. Gisin, *Nature (London)* **469**, 508 (2011).
- [23] F. Bussières, C. Clausen, A. Tiranov, B. Korzh, V. B. Verma, S. W. Nam, F. Marsili, A. Ferrier, P. Goldner, H. Herrmann, C. Silberhorn, W. Sohler, M. Afzelius, and N. Gisin, *Nat. Photonics* **8**, 775 (2014).
- [24] R. M. Macfarlane, *J. Lumin.* **100**, 1 (2002).
- [25] I. Usmani, M. Afzelius, H. de Riedmatten, and N. Gisin, *Nat. Commun.* **1**, 12 (2010).
- [26] C. O'Brien, N. Lauk, S. Blum, G. Morigi, and M. Fleischhauer, *Phys. Rev. Lett.* **113**, 063603 (2014).
- [27] L. A. Williamson, Y.-H. Chen, and J. J. Longdell, *Phys. Rev. Lett.* **113**, 203601 (2014).
- [28] A. Louchet, Y. Le Du, F. Bretenaker, T. Chanelière, F. Goldfarb, I. Lorgeré, J.-L. Le Gouët, O. Guillot-Noël, and P. Goldner, *Phys. Rev. B* **77**, 195110 (2008).
- [29] A. L. Alexander, J. J. Longdell, and M. J. Sellars, *J. Opt. Soc. Am. B* **24**, 2479 (2007).
- [30] E. Fraval, M. J. Sellars, and J. J. Longdell, *Phys. Rev. Lett.* **92**, 077601 (2004).
- [31] Ph. Goldner, O. Guillot-Noël, F. Beaudoux, Y. Le Du, J. Lejay, T. Chanelière, J.-L. Le Gouët, L. Rippe, A. Amari, A. Walther, and S. Kröll, *Phys. Rev. A* **79**, 033809 (2009).
- [32] E. Baldit, K. Bencheikh, P. Monnier, S. Briaudeau, J. A. Levenson, V. Crozatier, I. Lorgeré, F. Bretenaker, J. L. Le Gouët, O. Guillot-Noël, and Ph. Goldner, *Phys. Rev. B* **81**, 144303 (2010).
- [33] See Supplemental Material at <http://link.aps.org/supplemental/10.1103/PhysRevLett.114.170503> for the experimental determination of Nd^{3+} g tensor and hyperfine tensor.
- [34] O. Guillot-Noël, Ph. Goldner, Y. Le Du, E. Baldit, P. Monnier, and K. Bencheikh, *Phys. Rev. B* **74**, 214409 (2006).
- [35] E. R. Davies, *Phys. Lett. A* **47**, 1 (1974).
- [36] A. M. Tyryshkin, J. J. L. Morton, A. Ardavan, and S. A. Lyon, *J. Chem. Phys.* **124**, 234508 (2006).
- [37] R. Beach, M. D. Shinn, L. Davis, R. W. Solarz, and W. F. Krupke, *IEEE J. Quantum Electron.* **26**, 1405 (1990).
- [38] T. Böttger, C. W. Thiel, Y. Sun, and R. L. Cone, *Phys. Rev. B* **73**, 075101 (2006).
- [39] W. B. Mims, *Phys. Rev.* **168**, 370 (1968).
- [40] A. G. Maryasov, S. A. Dzuba, and K. M. Salikhov, *J. Magn. Reson.* **50**, 432 (1982).
- [41] Y. Kubo, C. Grezes, A. Dewes, T. Umeda, J. Isoya, H. Sumiya, N. Morishita, H. Abe, S. Onoda, T. Ohshima, V. Jacques, A. Dréau, J. F. Roch, I. Diniz, A. Auffèves, D. Vion, D. Esteve, and P. Bertet, *Phys. Rev. Lett.* **107**, 220501 (2011).
- [42] M. Hosseini, B. M. Sparkes, G. Campbell, P. K. Lam, and B. C. Buchler, *Nat. Commun.* **2**, 174 (2011).
- [43] M. P. Hedges, J. J. Longdell, Y. Li, and M. J. Sellars, *Nature (London)* **465**, 1052 (2010).
- [44] M. A. Nielsen and I. L. Chuang, *Quantum Computation and Quantum Information* (Cambridge University Press, Cambridge, England, 2000).
- [45] J. L. O'Brien, G. J. Pryde, A. Gilchrist, D. F. V. James, N. K. Langford, T. C. Ralph, and A. G. White, *Phys. Rev. Lett.* **93**, 080502 (2004).
- [46] S. Massar and S. Popescu, *Phys. Rev. Lett.* **74**, 1259 (1995).
- [47] A. Gilchrist, N. K. Langford, and M. A. Nielsen, *Phys. Rev. A* **71**, 062310 (2005).
- [48] S. Wimperis, *J. Magn. Reson.* **109**, 221 (1994).
- [49] G. T. Genov, D. Schraft, T. Halfmann, and N. V. Vitanov, *Phys. Rev. Lett.* **113**, 043001 (2014).